Atmos. Chem. Phys. Discuss., 8, 15491–15536, 2008
www.atmos-chem-phys-discuss.net/8/15491/2008/

Atmospheric Chemistry and Physics Discussions

This discussion paper is/has been under review for the journal *Atmospheric Chemistry and Physics (ACP)*. Please refer to the corresponding final paper in *ACP* if available.

Hydroxyl radicals in the tropical troposphere over the Suriname rainforest: airborne measurements

M. Martinez[1], H. Harder[1], D. Kubistin[1], M. Rudolf[1], H. Bozem[1], G. Eerdekens[1,*], H. Fischer[1], C. Gurk[1], T. Klüpfel[1], R. Königstedt[1], U. Parchatka[1], C. L. Schiller[2], A. Stickler[1,], J. Williams[1], and J. Lelieveld[1]**

[1]Department of Atmospheric Chemistry, Max Planck Institute for Chemistry, Mainz, Germany
[2]Department of Chemistry, York University, Toronto, Canada
[*]now at: Department of Biology, University of Antwerp, Belgium
[**]now at: Institute for Atmospheric and Climate Science, ETH Zürich, Switzerland

Received: 1 July 2008 – Accepted: 14 July 2008 – Published: 15 August 2008

Correspondence to: M. Martinez (martinez@mpch-mainz.mpg.de)

Published by Copernicus Publications on behalf of the European Geosciences Union.

Abstract

Direct measurements of OH and HO_2 over a tropical rainforest were made for the first time during the GABRIEL campaign in October 2005, deploying the custom-built HORUS instrument (HydrOxyl Radical measurement Unit based on fluorescence Spectroscopy), adapted to fly in a Learjet wingpod. Biogenic hydrocarbon emissions were expected to strongly reduce the OH and HO_2 mixing ratios as the air is transported from the ocean over the forest. However, surprisingly high mixing ratios of both OH and HO_2 were encountered in the boundary layer over the rainforest.

The HORUS instrumentation and calibration methods are described in detail and the measurement results obtained are discussed. The extensive dataset collected during GABRIEL, including measurements of many other trace gases and photolysis frequencies, has been used to quantify the main sources and sinks of OH. Comparison of these measurement-derived formation and loss rates of OH indicates strong previously overlooked recycling of OH in the boundary layer over the tropical rainforest, occurring in chorus with isoprene emission.

1 Introduction

The hydroxyl radical, OH, is the atmosphere's most important oxidizer and cleansing agent. The hydroperoxy radical, HO_2, is closely linked to OH in the atmosphere, and collectively they are referred to as HO_x. On a global scale, the main OH source in the lower troposphere is the photolysis of ozone producing an excited oxygen atom (O^1D), which subsequently reacts with water to produce two OH radicals (Levy, 1971). Another source of HO_x is the photolysis of formaldehyde, yielding two HO_2 radicals for each formaldehyde photolyzed (Sander et al., 2006). In addition, O_3 can react with terpenes yielding OH (Paulson and Orlando, 1996; Paulson et al., 1999). Since the latter source does not require photolysis, these reactions produce OH during day and night. On a diel average basis, however, photolytic sources are thought to contribute much more

ACPD

8, 15491–15536, 2008

to primary HO_x production than non-photolytic sources. The photolytic sources are especially strong in the tropics, where both humidity and irradiation intensity are high.

Once formed, OH and HO_2 undergo rapid reactions that lead to efficient interconversion between these radicals. OH reacts with CO or O_3 producing HO_2, and the oxidation of hydrocarbons by OH leads to the formation of peroxy radicals, RO_2, and HO_2. In the presence of NO, RO_2 is converted to HO_2, which reacts with NO or O_3 to recycle OH. The oxidation of hydrocarbons predominantly leads to the formation of formaldehyde (HCHO), increasing the source of HO_x. Tropical rainforests are a major source of volatile organic compounds (VOC) on a global scale, the dominant hydrocarbon being isoprene (Guenther et al., 1995). Isoprene and other VOC are very reactive towards OH and therefore air influenced by forest emissions can be expected to have a markedly different HO_x budget compared to both marine background and anthropogenically polluted air. The oxidation of large quantities of VOC over the rainforest, including isoprene, leads to the production of diverse organic RO_2 radicals.

The main sink of HO_x in the polluted boundary layer is the reaction of OH with NO_2 forming nitric acid, HNO_3. In air with low levels of nitrogen oxides, being predominant over the pristine rainforest, the reactions HO_2+HO_2 and HO_2+RO_2 are most important. These reactions form peroxides which are rapidly removed from the atmosphere by dry and wet deposition. Other sinks, such as radical deposition, heterogeneous chemistry on aerosols, multiphase cloud and rain chemistry and the formation of other chemical conmpounds such as pernitric acid are considered to be minor. Even though photolytic production of OH is highest in the tropics, over the rainforest a significant reduction of the oxidation capacity of the atmosphere is expected due to the strong emission of isoprene and other reactive organic species (e.g. Poisson et al., 2000; von Kuhlmann et al., 2004).

The GABRIEL campaign (Guyanas Atmosphere-Biosphere exchange and Radicals Intensive Experiment with the Learjet) took place in October 2005 in Suriname, to study the influence of tropical rainforests and their emissions on the atmospheric oxidation capacity (Lelieveld et al., 2008; Stickler et al., 2007; Eerdekens et al., 2008). A

ACPD
8, 15491–15536, 2008

suite of measurements relevant for studies of the photochemistry was performed using a Learjet 35A operated by the Gesellschaft für Flugzieldarstellung (GFD, Hohn, Germany). From the operational base, Johan A. Pengel International Airport in Zanderij, Suriname, 10 flights of about 3 h duration were performed between 3° N 59° W and 6° N 51° W. Air was sampled upwind of the forest over the tropical Atlantic Ocean to the east of French Guiana, and over the rainforest at various distances from the coast over French Guiana, Suriname and Guyana. The flight patterns were planned using chemical weather forecasts (Lawrence et al., 2003) and allowed for sampling both in the boundary layer (BL) and in the free troposphere (FT), generally starting with an ascent up to an altitude of 6.5 to 8 km a.s.l., followed by a descent into the BL at 300 to 600 m a.s.l., followed by alternating legs in the BL and the FT up to an altitude of about 3 to 3.5 km, and another ascent to levels above 6 km before landing.

2 Instrumentation

2.1 Measurement technique

OH and HO_2 were measured with the HORUS instrument (HydrOxyl Radical measurement Unit based on fluorescence Spectroscopy), which uses laser-induced fluorescence (LIF) of the OH molecule, based on the fluorescent assay by gas expansion (FAGE) technique originally proposed by Hard et al. (1984). HORUS was recently developed at our institute and adapted for measurements on the Learjet. The design of the detection module was originally based on ATHOS (Airborne Tropospheric Hydrogen Oxides Sensor), the Penn State HO_x instrument described by Faloona et al. (2004). The detection module, together with pumps and gas cylinders, was mounted in a wing-pod below the right wing, sampling the air directly from a forward-facing inlet to minimize surface effects (Fig. 1). From the laser system, similar to the one in ATHOS and mounted inside the Learjet cabin, the laser light was channeled to the detection module through 10 m optical fibers through the wing.

The air sample was drawn through a pinhole nozzle (1.25 mm diameter) into a reduced pressure detection chamber by a system consisting of a rotary vane vacuum pump (Leybold TRIVAC D25B) combined with a supercharger (Eaton M90). The constant volume flow of about 10 slm achieved with this pump system ensures an air speed through the detection area which is fast enough to exchange the air illuminated by the laser between two consecutive pulses to avoid possible laser-induced interferences. Different ambient pressures during flight lead to different internal pressures (2–5 hPa during GABRIEL), whereas the flow speed remains constant.

As the air flows through the laser beam, reflected in a White cell to cross the detection volume 32 times, the OH molecules are excited by laser pulses at 3 kHz at one of several vibronic transition lines near 308 nm ($A^2\Sigma - X^2\Pi$, $v'=\leftarrow v''=0$). The laser is tuned on and off resonance with the OH transition (called on-line and off-line) every 5 seconds to determine the OH fluorescence plus background signals and the background signals, respectively, resulting in a measurement time resolution of 10 s. During GABRIEL the UV laser power entering the White cell was usually in the range of 3 to 6 mW. The OH fluorescence extends beyond the prompt scattering (Rayleigh and wall scattering) and is detected with time-gated micro-channel plate detectors (Hamamatsu). The fluorescence decay is recorded with a time-resolution of 4 ns by a FPGA (field programmable gate array) and integrated for on- and off-line periods.

HO_2 is measured simultaneously in a second detection cell located 16 cm downstream of the first cell through quantitative conversion into OH by reaction with NO (nitric oxide, >99.5%), purified through a sodium hydroxidecoated silica (Sigma-Aldrich Ascarite) followed by LIF detection of OH. The NO is added through a loop between both cells and the NO flow is adjusted to achieve maximum yields of OH, which are reached at internal mixing ratios of about 0.1% of NO.

Various tests were conducted during flights to ensure that observed OH signals were not influenced by instrument artefacts. The addition of reagent NO to the system was occasionally interrupted to verify that HO_2 conversion does not take place in the OH detection cell. Scans of 0.1 nm of the OH spectrum conclusively showed that the ob-

ACPD
8, 15491–15536, 2008

served signal was produced by OH. To test for laser-generated OH, the laser power was occasionally quickly reduced by 50%; a laser-generated signal would decrease quadratically, the measured signal however always decreased proportionally, indicating the absence of laser-induced interference.

The precision derived from the noise of the on- and off-line signals during the GABRIEL campaign was about 7% for OH and 1% for HO_2.

2.2 Shrouded inlet

A front-facing shrouded inlet was designed to sample air directly into the wingpod and to allow for in-flight calibrations to complement the more extensive and thorough calibrations performed on the ground before and after each flight.

The design was based on the shrouded inlet described by Eisele et al. (1997). Our inlet consists of a shroud for alignment of the incoming air flow and only one tube ending with a deflector plate with a 90% blockage to decelerate the air. The original design was further adapted for integration into the wingpod using an outlet vent system at the sides of the wingpod. To allow for in-flight calibrations, a Hg lamp (LOT-Oriel Pen-Ray) was included in the assembly, the output of which was monitored by 2 phototubes, one attached directly to the lamp housing, the other at the far side of the inlet tube. The air speed within the inlet was monitored with a Pitot tube behind the nozzle.

Computational Fluid Dynamics calculations of air within the shrouded inlet were performed by P. Lucas, S. van Zuijlen and H. Bijl (Delft University of Technology, The Netherlands). The numerical results from these calculations indicate that our inlet assembly is capable of decelerating free stream velocities up to 200 m/s to a value lower than 20 m/s in the calibration section just in front of the sampling orifice, while maintaining a smooth flow, thus preventing vortices causing OH radical loss on the inlet walls (Fig. 2). The reduction of stream velocity is necessary for the in-flight calibration, to produce sufficient OH through the extended irradiation of the air by the Hg lamp. Calculations at an angle of attack other than zero show that the geometry of the wingpod with the inlet is capable of maintaining a smooth and attached flow even when the

free-stream flow is deflected by up to 15 degrees.

The ultimate test of the adequacy of the inlet for OH sampling was provided by the measurements made with this inlet during test flights and also during the GABRIEL campaign. The average angles flown by the Learjet during the GABRIEL flight were (5±3)° pitch and (0±7)° roll angle. Fast changes higher than 10° in pitch and 20° in roll angle within the 10 s resolution of the OH data do not lead to significant changes in the measured OH mixing ratios (Fig. 3).

2.3 Calibration

The instrument was calibrated thoroughly before or after each flight. In addition, relative calibrations took place during the flights to verify that different flight conditions did not have unexpected effects on the sensitivity.

The ground calibration technique is based on the method described by Faloona et al. (2004). A measured amount of air flows through the calibrator, a square aluminum tube, 16 mm wide and high. Water vapour is added to the air upstream of the flow tube and measured with an IR absorption instrument (LI-COR LI-7000), which is calibrated against a LI-COR dew point generator (LI-610). A Hg lamp, attached to the tube over a window, serves as a photolysis source for water vapour, producing equal amounts of OH and HO_2:

$$H_2O + h\nu(184.9\,\text{nm}) \rightarrow OH + H, \quad \text{(R1.1)}$$

$$H + O_2 \rightarrow HO_2. \quad \text{(R1.2)}$$

The lamp flux is calibrated by N_2O photolysis (see Sect. 2.3.1 below). The overlap between the lamp flux field and the airflow field is calculated to determine the exposure time of the water vapour molecules to the 184.9 nm flux.

ACPD
8, 15491–15536, 2008

The concentration of OH is thus given by

$$[OH]=[HO_2]=\Phi_0\,\sigma_{H_2O}[H_2O]t\,f_{O_2}, \quad (1)$$

where Φ_0 is the photon flux, σ_{H_2O} is the absorption cross section of H_2O at 184.9 nm, and t is the exposure time. f_{O_2} is a correction factor to account for flux reduction through absorption by O_2 across the tube height h according to Lambert-Beer's law:

$$f_{O_2}=\frac{\Phi}{\Phi_0}=\frac{\int_0^h e^{-\sigma_{O_2}[O_2]x}dx}{h}. \quad (2)$$

The tube's outlet is placed near the instrument's inlet and the airflow set to 50 slm, such that the flow in the tube is turbulent (Reynolds number of 3500) with a flat velocity profile. The calibration flow is several times greater than the sampling flow of the instrument, overfilling the volume around the instrument nozzle to ensure that no ambient air is mixed in. Wall loss of OH radicals within the calibration tube between the lamp and the instrument inlet was 8%. The photon flux reduction due to O_2 absorption was 5%.

2.3.1 Determination of the photon flux of the mercury lamp

The photon flux of the Hg lamp was determined in the laboratory directly before and after the campaign through N_2O actinometry measurements in nitrogen and helium, similar to the calibration procedure described by Edwards et al. (2003). N_2O photodissociates at 184.9 nm producing the excited oxygen atoms $O(^1D)$

$$N_2O+h\nu \rightarrow O(^1D)+N_2, \quad (R2)$$

which is then collisionally quenched or reacts with N_2 or N_2O (Sander et al., 2006):

ACPD
8, 15491–15536, 2008

$$O(^1D)+N_2+M \rightarrow N_2O, \quad \text{(R3.1)}$$

$$O(^1D)+N_2 \rightarrow O(^3P)+N_2, \quad \text{(R3.2)}$$

$$O(^1D)+N_2O \rightarrow N_2+O_2, \quad \text{(R3.3)}$$

$$O(^1D)+N_2O \rightarrow 2NO, \quad \text{(R3.4)}$$

$$O(^1D)+N_2O \rightarrow O(^3P)+N_2O. \quad \text{(R3.5)}$$

The quenching reaction (R3.5) is negligible compared to the other reactions (Vranckx et al., 2008).

The flux can be calculated from the NO concentrations produced by irradiating defined mixtures of N_2O in a carrier gas:

$$\Phi_0 = \frac{(k_1[N_2][M]+k_2[N_2]+k_3[N_2O]+k_4[N_2O])[NO]}{2k_4[N_2O]^2\sigma_{N_2O}f_{N_2O}t}, \quad (3)$$

where Φ_0 is the actinic flux from the lamp, σ_{N_2O} is the absorption cross section of N_2O at 184.9 nm, and f_{N_2O} is a correction factor to account for flux reduction through absorption by N_2O.

The NO produced was measured using a TECO 42C (Thermo Environmental Instruments Inc.). In order to produce NO concentrations well above the detection limit of 50 ppt (pmol/mol), N_2O (Messer, 100% UHP) was mixed into flows between 5 and

35 slm to obtain various mixing ratios of 0–100%. N_2 or He was used as carrier gas. The benefit of using helium is the absence of the reactions (R3.1) and (R3.2) and therefore a better signal to noise ratio, as $O(^1D)$ reaction with He is very slow (Preston and Cvetanovic, 1966). However, due to the lower density and viscosity of helium, it becomes more difficult to achieve a turbulent flow with helium. To ensure a flat velocity profile of the N_2O flow under all conditions considered, a flat 3 mm high photolysis chamber was employed (Fig. 4). Under these conditions, the flux reduction due to N_2O absorption was up to f_{N_2O}=0.6 depending on the N_2O mixing ratio used. Depending on the flow through the photolysis chamber the inside pressure is higher than the ambient pressure, which needs to be taken into account.

The results of the laboratory measurements are shown in Fig. 5. The photon fluxes measured using different carrier gases all agree within the respective uncertainties, showing no dependency on the gas flow or on the fraction of N_2O in the gas mixture. Model simulations (Comsol, Femlab v3.1) indicate a turbulent flow in the photolysis chamber for a flow of 7 slm N_2. The agreement of the measured photon fluxes confirms that the flow was turbulent under all conditions.

The systematic error of the lamp photon flux is a result of all uncertainties listed in Table 1 and is estimated to be 12%.

Ideally the photon flux should be measured in the tube used for calibration of the LIF instrument and with the same gas flows. The high flow rate of 50 slm, however, leads to low NO yields from N_2O photolysis, which were difficult to quantify with the routinely used TECO NO analyzer. A comparison of flux measurements performed with the calibration tube, sampling NO with a more sensitive CLD-780TR (Eco Physics AG) instrument through a 1/8" Teflon tube integrated into a modified LIF instrument nozzle, is shown in Fig. 6 and shows reasonable agreement.

2.3.2 Ground calibration

The sensitivity of the LIF-FAGE instrument is influenced by the amount of water vapour and the pressure within the detection cell (Faloona et al., 2004). H_2O as well as N_2

and O_2 reduce the fluorescence signal by collisional quenching of the excited states of OH, which also depends on temperature. Therefore the LIF signal S is a function of the laser light power P in the detection cell, the water mixing ratio, the temperature T and the density ρ.

The changing pressures at different altitude levels during the flights were simulated on the ground by applying various nozzle diameters (0.7 mm to 1.5 mm) to the inlet, producing pressures between 1.9 and 8.2 hPa in the detection volume during calibration, fully covering the range of pressures of 2 to 5 hPa registered during flights.

During the GABRIEL campaign, the influence of quenching was not sufficient to explain the sensitivity dependency on water mixing ratio, possibly due to wall loss effects on the Teflon-coated inlet tube. The parameterization for the sensitivity dependencies characterized on the ground was improved by including additional dependencies on water mixing ratio in 1st order and on density in 2nd order:

$$C(P, H_2O, T, \rho) = C_0 P [a_0 + a_1 \rho + a_2 \rho^2][1 + a_3 H_2O] Q(\rho, T, H_2O), \quad (4)$$

where the parameters C_0, dependent on the optics and the detector sensitivity, and a_0, a_1, a_2, a_3 are determined from best fits to the ground calibration data.

The quenching factor Q is given by Faloona et al. (2004)

$$Q(\rho, T, H_2O) = \frac{1}{\Gamma}\left(e^{-\Gamma g_1} - e^{-\Gamma g_2}\right), \quad (5)$$

where $\Gamma(\rho, T, H_2O)$ is the excited state decay frequency, and g_1 and g_2 are the detector gate opening and closure times after excitation by the laser pulse.

Ground calibrations were performed after each flight, an example of which is shown in Fig. 7. The dependencies on pressure, temperature and humidity are expected to remain constant throughout the campaign, thus the parameters a_0–a_3 were the same for all calibrations performed. The parameter C_0, however, was allowed to vary for each calibration due to problems with the pump setup during GABRIEL, which occasionally led to contamination of the optical components with rotary pump oil vapour during

shutdown of the instrument. The resulting sensitivity coefficients for each flight day are plotted in Fig. 8.

The 1σ uncertainty for OH and HO_2 resulting from the density dependency was 6% and 9%, for the water dependency 5% and 7%, whereas the standard deviation of C_0 is 16% and 17%, respectively. The error of the quenching factor Q was negligible as long as humidity data was available. When it was not (58% of the data, including all of flights #2 and #7), the mean atmospheric absolute humidity profile observed during the GABRIEL campaign was used instead, leading to an additional systematic error of 2.6% on average and always below 7% for all data involved.

2.3.3 In-flight calibration

The calibration during flight complements the more time-intensive and therefore more accurate ground calibration, checking the dependencies found on the ground against sensitivity changes during flight. Like the ground calibration, the in-flight calibration is based on photolysis of atmospheric water vapour, and the OH-concentration produced during the in-flight calibrations is a function of the photon flux, the water concentration and the air speed (see Eq. 1). Whereas a relative calibration is sufficient for the purpose of in-flight calibration, a detailed knowledge of the lamp flux field from the Hg lamp installed in the shrouded inlet and the speed in the irradiated area is not necessary and only relative changes during the flight are monitored.

Due to technical problems with the phototubes it was not possible to monitor the photon flux from the lamp during the GABRIEL campaign, and we assume the intensity was constant throughout the campaign. This is reasonable since the lamp was heated and remained at (20±10)°C during the flights.

The air speed in the area irradiated by the lamp is not the same as measured by the Pitot tube behind the instrument nozzle, but the ratio of these two air speeds should be constant at all speeds and altitude levels and even at all pitch angles flown. This assumption is supported by air flow simulations (Fig. 2). Calibrations were performed while the aircraft was flying straight at constant flight levels.

ACPD
8, 15491–15536, 2008

The atmospheric water vapour concentration was measured with the FABLE instrument (Fast AirBorne Licor Experiment, NDIR absorption spectrometer; Gurk et al., 2008).

OH was produced during calibration periods of about 2 min. It was not possible to produce HO_2 in significant amounts compared to atmospheric mixing ratios, usually being a factor 10 to 100 higher than OH in the troposphere. As the lamp produces equal amounts of OH and HO_2, the additional signal was usually larger than the atmospheric OH signal, but small compared to atmospheric HO_2. Therefore the in-flight calibration was used only to characterize the OH sensitivity of the instrument.

OH signals observed during the in-flight calibration are evaluated using the sensitivity calculated according to the ground calibration and compared to the OH concentrations produced. Figure 9 presents the results for all in-flight calibrations of the entire campaign, which show considerable scatter. However, the scatter is not random, but follows different slopes during individual flights. The most likely explanation is contamination of the optical components with oil vapour, which occasionally occurred during shutdown, changing the instrument sensitivity constant C_0 between the flight and the ground calibration performed afterwards. The in-flight calibrations can thus be used to derive correction factors for the ground calibrations. Application of these correction factors bring the in-flight calibrations into agreement by modifying the slope derived from all calibrations of each flight to an average slope of all calibrations performed during the campaign.

$$C_0^* = \frac{m_i}{\overline{m}} C_0 \tag{6}$$

For HO_2 the ground calibration parameters were used without correction, as the in-flight calibrations were not adequate for HO_2. The same holds for OH measured on flights #2 and #7, as no H_2O data is available for these flights and the in-flight calibrations could therefore not be evaluated.

The 1σ standard deviation of the corrected sensitivity constants C_0^* for OH is 12%. The variability of the correction factors m_i is much larger: 26%. The latter value is used

as an error estimate for the sensitivity constant C_0 for HO_2 and for OH during flights #2 and #7, when in-flight calibration was not available. Together with the uncertainties for the sensitivity dependencies on density, humidity and quenching discussed above, this leads to a total accuracy of our measurements (2σ) of approximately 40% for OH for all data except for flights #2 and #7, and 60% for OH on these flights and for the HO_2 data. The overall precision and accuracy of the HO_x measurements during GABRIEL is summarized in Table 2.

The in-flight calibrations with the corrected sensitivity constants C_0^* are shown in Fig. 10. Two different regimes are now apparent, with higher sensitivity in conditions where less OH is produced by the in-flight calibrator, which is the case at higher altitudes due to lower ambient humidity. The two sensitivity regimes separate conditions which differ in altitude (below and above 2000 m a.s.l.), ambient water mixing ratio (above and below 1.5%), ambient pressure and temperature, and atmospheric layer (boundary layer and free troposphere). The instrument sensitivity appears to be almost twice as high in the free troposphere compared to the boundary layer. We cannot discern if the reason is indeed a change in instrument sensitivity either not characterized or incorrectly characterized by the ground calibration, or an underestimation of the OH produced during calibration at higher altitudes, e.g. due to variations in lamp flux or condensation on the windows, or an overestimation at lower altitudes. If the discrepancy is due to an under- or overestimation of the OH produced during calibrations and not to a real change in instrument sensitivity, our evaluation is correct. If instead there is a real change in instrument sensitivity not characterized by the ground calibration, we either overestimate OH and possibly also HO_2 in the free troposphere (if the ground calibration is more representative for the sensitivity in the boundary layer) and/or underestimate them in the boundary layer by up to a factor 2.

2.3.4 Interferences

Likely interferences from compounds either fluorescing at similar wavelengths as OH or producing OH within the instrument have been examined in detail for the Penn-State

ATHOS instrument, on which the detection unit of our HORUS instrument is based (Ren et al., 2004). Beside a negative interference from naphthalene, no significant interference was found for any of the examined compounds at atmospheric mixing ratios, including ozone, hydrogen peroxide, formaldehyde, sulfur dioxide, nitrous acid, nitric acid, organic peroxy radicals and various VOC including isoprene.

3 Results and discussion

3.1 HO_x mixing ratios, diurnal variation and spatial distribution

OH and HO_2 were measured during all flights starting from flight #2. Over the forest and especially in the boundary layer a strong influence from biogenic hydrocarbon emissions such as isoprene was expected. Most of these hydrocarbons are emitted in reduced forms containing one or more double bonds and hence should react rapidly with OH. Therefore model calculations generally predict very low OH and HO_2 mixing ratios in the boundary layer over large rainforest areas (Poisson et al., 2000; von Kuhlmann et al., 2004; Lelieveld et al., 2008).

Forest emissions of hydrocarbons have previously been shown to be both temperature and light dependent (Guenther et al., 1995). Therefore the VOC composition over the forest is likely to vary with the time of day. To study the influence of forest emissions on the HO_x budget, all data was binned for morning, noon and afternoon hours, separately for measurements over the forest and over the ocean. The "morning" dataset includes all measurements between 08:00 and 11:00 local time (UTC-3), "noon" between 11:00 and 14:00, and "afternoon" between 14:00 and 17:00. All data for which topographical elevation is absent (0 m a.s.l.) is considered to be over the ocean, whereas data taken west of 52°30′ W and south of 5°39′ S is considered to be over the forest (see map in Fig. 14); data measured between the coastline and the forest data boundaries, amounting to about 9% of all data, was not taken into account.

OH mixing ratios varied between 0.25 ppt in the morning and up to 0.75 ppt around

ACPD
8, 15491–15536, 2008

noon, when photolytic production is highest (Fig. 11). Maximum mixing ratios of OH were encountered at about 2 to 3 km altitude a.s.l., decreasing towards higher altitudes and in the boundary layer. The decrease in the boundary layer is strongest over the forest around noon, where on average 0.25 ppt were observed at 500 m a.s.l. over the forest, compared to 0.5 ppt at the same altitude over the ocean. However, the mixing ratios encountered over the forest canopy were still much higher than predicted by chemical transport and box models, which typically calculate less than 10^6 molecules/cm^3 or 0.04 ppt OH in the boundary layer (Lelieveld et al., 2008; Butler et al., 2008; Kubistin et al., 2008).

The HO_2 vertical profiles observed over the ocean and over the forest were quite similar in the free troposphere, showing decreasing mixing ratios with increasing altitude above 2 to 3 km a.s.l., and reaching up to 40 ppt at 2 km a.s.l. (Fig. 11). In the boundary layer the picture is rather different: whereas over the ocean HO_2 increases with altitude together with OH, over the forest HO_2 is significantly more abundant. HO_2 in the forest boundary layer accordingly increases only slightly with increasing altitude in the morning. At noon, average mixing ratios of 55 ppt were observed at the lowest flight levels, and somewhat lower mixing ratios of around 50 ppt in the afternoon, decreasing with altitude.

The main primary source of HO_x is the photolysis of ozone and subsequent reaction with water. Mainly due to changing photolysis rates, this source varies strongly, usually more than the sum of the sinks of OH. Therefore, a linear correlation of OH with the OH production rate from ozone photolysis is expected (Holland et al., 2003). In environments with low concentrations of NO, the cycling of HO_2 to OH is limited. The dominant sink of HO_2 under these conditions is the self-reaction and the reaction with organic peroxy radicals, leading to a correlation between HO_2 and the square root of the production rate. OH concentrations observed in the free troposphere between 3000 and 5000 m a.s.l. both over the ocean and over the forest and in the boundary layer over the ocean all show the expected linear correlation (Fig. 12). By plotting mixing ratios rather than concentrations versus production rates, the slopes are comparable

despite the different altitude ranges. The OH mixing ratio in the boundary layer over the forest shows only a weak correlation with the OH production rate (R^2=0.19), compared to R^2=0.69, 0.47 and 0.48 in the free troposphere over the ocean and over the forest and in the boundary layer over the ocean, respectively. For HO_2 the correlation with the square root of the OH production rate is also lower in the boundary layer over the forest, with R^2=0.24 compared to 0.59, 0.53 and 0.76 in the free troposphere over the ocean and over the forest and in the boundary layer over the ocean, respectively (Fig. 12).

A strong dependency of OH and HO_2 on the time of day is also to be expected. Indeed, the highest mixing ratios of about 0.7 ppt OH were found around 12:30 local time in the free troposphere, independent of location (Fig. 13). This diurnal variation, however, was absent in the boundary layer over the forest, where observed mixing ratios scattered around 0.1 to 0.5 ppt throughout the day with no discernible temporal dependency. In contrast, the daytime maximum of HO_2 in the forest boundary layer, which is reached later in the afternoon at around 14:00 LT, was enhanced by about a factor 2 in the forest boundary layer compared to that over the ocean.

Thus our measurements show that, when an air parcel is transported through the boundary layer over the rainforest and entrains biogenic emissions, OH decreases whereas HO_2 increases. The VOC emissions from the rainforest as well as their photochemical products can be expected to affect the HO_x mixing ratios. If the hydrocarbon emissions and their secondary products accumulate in the air as it is being transported over the forest, then HO_x mixing ratios measured at the same time of day should change consistently with distance from the coast. However, no such trend is discernible from our data. Instead the coastline quite clearly separates the two concentration regimes: OH decreases and HO_2 increases abruptly at the coastline (Fig. 14), and VOC accumulation either does not occur or has no significant photochemical consequencies. The data rather suggests that the VOC emissions mixed into the boundary layer instantaneously affect HO_x. This indicates that the compounds influencing HO_x are relatively short-lived, with a lifetime of the order of the boundary layer mixing time

scale, which is about an hour or less (Eerdekens et al., 2008; Ganzeveld et al., 2008).

3.2 HO_x sources

O_3, NO, the sum of H_2O_2 and organic peroxides and the photolysis frequency of NO_2 were all measured during the GABRIEL campaign. Other photolysis frequencies apart from J_{NO_2} were calculated with the radiative transport model TUV v4.1 (Tropospheric Ultraviolet-Visible Model; Madronich and Flocke, 1998) and scaled to the ratio of measured to calculated NO_2 photolysis frequencies.

Thus the main sources of OH can be calculated from the measured data. The dominant OH source in the troposphere up to 6 km a.s.l. is the photolysis of ozone and the reaction of $O(^1D)$ with water (Fig. 15). At higher altitudes and lower humidity the photolysis of peroxides becomes more important. Conversion of HO_2 to OH through reactions with NO and O_3 also contribute substantially in the upper troposphere, and in the morning also in the boundary layer.

Most of the primary HO_x production is production of OH, amounting to up to 2×10^7 molecules/cm^3/s. Production of HO_2 from photolysis of formaldehyde is much less amounting up to 3×10^6 molecules/cm^3/s.

The source terms are actually quite similar when comparing air over the forest and over the ocean. Only the conversion of HO_2 to OH through reaction with NO is more important over the forest, mostly due to NO emissions from the soil (Ganzeveld et al., 2008). OH production due to O_3 photolysis decreases in the boundary layer mainly because ozone mixing ratios also decrease from (40±10) ppb at 2 to 3 km to (17±4) ppb within the lowest 1000 m a.s.l., with slightly higher values over the forest than over the ocean (Stickler et al., 2007). At higher altitudes the OH production rate decreases due to the declining absolute humidity.

3.3 OH sinks

The Learjet payload included measurements of the main reactants of OH, including isoprene and its reaction products methacrolein (MACR) and methyl vinyl ketone (MVK). The OH reactivity, which is the inverse of the OH lifetime, can therefore be derived from the sum of the reaction rate coefficients times the measured reactant concentrations. The altitude profiles of the OH reactivity over the forest and over the ocean are compared in Fig. 16. Over the ocean isoprene, methacrolein and MVK are below the detection limit and the total reactivity is below 1 s^{-1}, decreasing further at higher altitudes. CO is the main reactant with OH at all altitudes, contributing more than half of the total reactivity, followed by methane, formaldehyde and O_3. Over the forest, these four species give rise to reactivities of up to 1.2 s^{-1} in the boundary layer, somewhat higher than over the ocean due to higher CO and formaldehyde mixing ratios (Stickler et al., 2007). The total OH reactivity, however, is clearly dominated by isoprene, contributing about 75% of the total reactivity of 7 to 9 s^{-1} in the boundary layer. In the free troposphere, OH reactivities are similar over the forest and over the ocean.

3.4 OH steady state

According to the OH reactivities derived in the previous section, OH lifetimes vary between 0.1 s in the forest boundary layer and a few seconds in the upper troposphere. OH concentrations therefore adjust rapidly to changing conditions in an air mass reaching steady state, where OH production and destruction balance. Total OH destruction can be calculated from measured OH concentrations and reactivities and compared to the total production.

OH production and destruction generally agree within the uncertainty and the variability of the observations (Fig. 17). However, they differ significantly in the forest boundary layer at noon and in the afternoon. Here the OH destruction derived from trace gas observations strongly exceeds the production due to much higher sinks compared to the morning hours, whereas the sources do not change as much throughout

the day. At noon and in the afternoon OH destruction in the forest boundary layer based on measured trace gases is about 5×10^7 molecules/cm^3/s, pointing towards additional unaccounted for production mechanisms which are about 4 times larger than the known OH sources. The missing production thus correlates with the main sinks, indicating additional OH recycling rather than primary sources. The most important sink of OH in the forest boundary layer, as shown in the previous section, is the reaction with isoprene. This compound is emitted by the vegetation depending on light and temperature (Guenther et al. 1991), and during the GABRIEL campaign isoprene concentrations were usually higher later in the day following the increase in temperature (Fig. 18). Additional recycling of OH related to isoprene chemistry is therefore most likely to resolve the discrepancy between OH production and destruction found during GABRIEL (see also Lelieveld et al., 2008).

4 Conclusions

While here we present the first OH measurements from the boundary layer over the pristine (low-NO) tropical rainforest, there is some previous experimental evidence which has suggested a higher oxidation capacity in the forested boundary layer than predicted by models. Thornton et al. (2002) suggested a reduction of the HO_x chain termination reaction of HO_2 with RO_2 yielding ROOH by about a factor of 10 in order to explain measurements in Nashville, Tennessee, in a suburban environment with a high biogenic VOC load. Kuhn et al. (2007) indirectly inferred a range of OH concentrations during daytime of 3–8×10^6 cm^{-3} from vertical gradients of isoprene, methyl vinyl ketone and methacrolein in Brazil. Ren et al. (2008) measured OH over North America and found that the observed-to-modeled OH ratio in the planetary boundary layer in forested regions is a strong function of isoprene. Furthermore, atmospheric chemistry-transport models tend to strongly overestimate isoprene in the boundary layer over forests, consistent with an underestimate of OH. To get around this problem, isoprene sources have been reduced in models by a factor of two or more (von Kuhlmann et

al., 2004; Jöckel et al., 2006). The measurements presented here are the first direct evidence of a higher than predicted oxidation capacity over tropical rainforests and its link to the rainforest emissions of isoprene.

The possibility of a measurement error needs to be addressed. Likely interferences from other compounds present in the atmosphere have been examined in detail for the Penn-State ATHOS instrument, on which the detection unit of our HORUS instrument is based (Ren et al., 2004). Even though significant interferences can be excluded for many compounds, including isoprene, the possibility of interference from an unidentified compound present over the rainforest cannot be completely ruled out. The good agreement of measured OH with the expected steady state conditions over the ocean and in the free troposphere corroborates the absence of instrumental problems under a wide range of conditions, including temperature, humidity and pressure variations from the tropical boundary layer to the upper troposphere. Therefore any hypothetical interference would have to be related to a trace gas present only in the forest boundary layer. Furthermore, it should be emphasized that HO_2 mixing ratios were also greatly enhanced over the rainforest. As mixing ratios of HO_2 are typically 2 orders of magnitude higher than OH, an interference for HO_2 as well as for OH would require the OH interference signal to be enhanced by 2 orders of magnitude when the sampled air is mixed with high concentrations of NO in the instrument for conversion of HO_2 to OH.

The total OH reactivity derived in this work is based on the limited set of hydrocarbon measurements on the Learjet. Other hydrocarbon species emitted by the forest but not measured are likely to further increase the total OH reactivity, e.g. the monoterpenes (DiCarlo et al., 2004; Williams et al., 2007). Measurements of total OH reactivity were not performed on the Learjet, although a limited dataset is available from within the canopy on Brownsberg, a ground site close to our operational base in central Suriname (Sinha et al., 2008). These measurements show very high reactivities, of the order of $100\,s^{-1}$. It may be speculated that within the canopy a large variety of hydrocarbons emitted by the rainforest is present, including e.g. sesquiterpenes, many of which are highly reactive and therefore short-lived. These species are unlikely to survive long

enough to play a significant role even at the lowest altitudes sampled with the Learjet (around 300 m a.s.l.), though they could be important for HO_x concentrations within the canopy, possibly providing an OH source through ozonolysis as well as an OH sink. Measurements of HO_x and OH reactivity within the rainforest canopy will be crucial to unravel the intriguing atmospheric chemistry of the rainforest ecosystem.

Missing OH production has been found to be about 4 times larger than the sum of known OH sources in the rainforest boundary layer and to correlate with isoprene emissions. While the existence of primary sources, e.g. ozonolysis of reactive hydrocarbons emitted together with isoprene, cannot be ruled out, the possibility of unknown reactions recycling OH at some intermediate step of isoprene chemistry is a more straightforward explanation. This hypothesis is further discussed in other papers of the GABRIEL special issue through comparison of the measurements presented here with the results of a box model (Kubistin et al., 2008) and of a global chemistry-climate model (Butler et al., 2008).

Acknowledgements. The first deployment of our instrument on aircraft would not have been possible without the invaluable support provided by Enviscope GmbH (Frankfurt, Germany) and the technicians of the GFD (Gesellschaft für Flugzieldarstellung, Hohn, Germany) during integration into the Learjet, the conduction of test-flights prior to and during the GABRIEL campaign. We also wish to thank the pilots of the GFD for their engagement in the design of unconventional flight plans and their realization. Further, we thank Tim Butler and Mark Lawrence for their contribution in planning the flight tracks during the campaign using chemical weather forecasts, as well as helpful discussions on the results of global model simulations.

The publication of this article is financed by the Max Planck Society.

References

Butler, T., Taraborrelli, D., Brühl, C., Fischer, H., Harder, H., Martinez, M., Williams, J., Lawrence, M., and Lelieveld, J.: Improved simulation of isoprene oxidation chemistry with the ECHAM5/MESSy chemistry-climate model: Lessons from the GABRIEL airborne field campaign, Atmos. Chem. Phys., 8(16), 4529–4546, 2008.

Di Carlo, P., Brune, W. H., Martinez, M., Harder, H., Lesher, R., Ren, X., Thornberry, T., Carroll, M. A., Young, V., Shepson, P. B., Riemer, D., Apel, E., and Campbell, C.: Missing OH reactivity in a forest: Evidence for unknown reactive biogenic VOCs, Science, 304, 722–725, 2004.

Edwards, G. D., Cantrell, A. C., Stephens, S., Hill, B., Goyea, O., Shetter, R. E., Mauldin, R. L., Kosciuch, E., Tanner, D., and Eisele, F. L.: Chemical ionization mass spectrometer instrument for the measurement of tropospheric HO_2 and RO_2, Anal. Chem., 75, 5312-5327, 2003.

Eerdekens, G., Ganzeveld, L., Vil-Guerau de Arellano, J., Klpfel, T., Sinha, V., Yassaa, N., Williams, J., Harder, H., Kubistin, D., Martinez, M., and Lelieveld, J.: Flux estimates of isoprene, methanol and acetone from airborne PTR-MS measurements over the tropical rainforest during the GABRIEL 2005 campaign, Atmos. Chem. Phys. Discuss., 8, 12 903–12 969, 2008.

Eisele, F. L., Mauldin III, R. L., Tanner, D. J., Fox, J. R., Mouch, T., and Scully, T.: An inlet/sampling duct for airborne OH and sulfuric acid measurements, J. Geophys. Res., 102, 27 993–28 001, 1997.

Faloona, I. C., Tan, D., Lesher, R. L., Hazen, N. L., Frame, C. L., Simpas, J. B., Harder, H., Martinez, M., DiCarlo, P., Ren, X., and Brune, W. H.: A laser induced fluorescence instrument for detecting tropospheric OH and HO_2: Characteristics and calibration, J. Atmos. Chem., 47, 139–167, 2004.

Ganzeveld, L., Eerdekens, G., Feig, G., Fischer, H., Harder, H., Königstedt, R., Kubistin, D., Martinez, M., Meixner, F. X., Scheeren, B., Sinha, V., Taraborrelli, D., Williams, J., Vilà-Guerau de Arellano, J., and Lelieveld, J.: Surface and boundary layer exchanges of volatile organic compounds, nitrogen oxides and ozone during the GABRIEL Campaign, Atmos. Chem. Phys. Discuss., 8, 11 909–11 965, 2008.

Guenther, A. B., Monson, R. K., and Fall, R.: Isoprene and monoterpene emission rate variability observations with eucalyptus and emission rate algorithm development, J. Geophys.

Res., 96, 10 799–10 808, 1991.
Guenther, A., Nicolas Hewitt, C., Erickson, D., Fall, R., Geron, C., Graedel, T., Harley, P., Klinger, L., Lerdau, M., McKay, W. A., Pierce, T., Scholes, B., Steinbrecher, R., Tallamraju, R., Taylor, J., and Zimmerman, P.: A global model of natural volatile organic compound emissions, J. Geophys. Res., 100, 8873–8892, 1995.
Gurk, C., Fischer, H., Hoor, P., Lawrence, M. G., Lelieveld, J., and Wernli, H.: Airborne in-situ measurements of vertical, seasonal and latitudinal distributions of carbon dioxide over Europe, Atmos. Chem. Phys. Discuss., 8, 7315–7337, 2008, http://www.atmos-chem-phys-discuss.net/8/7315/2008/.
Hard, T. M., O'Brien, R. J., Chan, C. Y., and Mehrabzadeh, A. A.: Tropospheric free radical determination by FAGE, Environ. Sci. Technol., 18, 768–777, 1984.
Holland, F., Hofzumahaus, A., Schäfer, J., Kraus, A., and Pätz, H. W.: Measurements of OH and HO_2 radical concentrations and photolysis frequencies during BERLIOZ, J. Geophys. Res., 108, 8246 pp., doi:10.1029/2001JD001393, 2003.
Jöckel, P., Tost, H., Pozzer, A., Brühl, C., Buchholz, J., Ganzeveld, L., Hoor, P., Kerkweg, A., Lawrence, M. G., Sander, R., Steil, B., Stiller, G., Tanarhte, M., Taraborrelli, D., van Aardenne, J., and Lelieveld, J.: The atmospheric chemistry general circulation model ECHAM5/MESSy, Consistent simulation of ozone from the surface to the mesosphere, Atmos. Chem. Phys., 6, 5067–5104, 2006, http://www.atmos-chem-phys.net/6/5067/2006/.
Kubistin, D., Harder, H., Martinez, M., Rudolf, M., Sander, R., Bozem, H., Eerdekens, G., Fischer, H., Gurk, C., Klüpfel, T., Königstedt, R., Parchatka, U., Schiller, C., Stickler, A., Taraborrelli, D., Williams, J. and Lelieveld, J.: Hydroxyl Radicals in the Tropical Troposphere over the Suriname Rain Forest: Comparison of Measurements with the Box Model MECCA, Atmos. Chem. Phys., accepted, 2008.
Kuhn, U., Andreae, M. O., Ammann, C., Araújo, A. C., Brancaleoni, E., Ciccioli, P., Dindorf, T., Frattoni, M., Gatti, L. V., Ganzeveld, L., Kruijt, B., Lelieveld, J., Lloyd, J., Meixner, F. X., Nobre, A. D., Pöschl, U., Spirig, C., Stefani, P., Thielmann, A., Valentini, R., Kesselmeier, J.: Isoprene and monoterpene fluxes from Central Amazonian rainforest inferred from tower-based and airborne measurements, and implications on the atmospheric chemistry and the local carbon budget, Atmos. Chem. Phys. 7, 2855–2879, 2007.
Lawrence, M. G., Rasch, P. J., von Kuhlmann, R., Williams, J., Fischer, H., de Reus, M., Lelieveld, J., Crutzen, P. J., Schultz, M., Stier, P., Huntrieser, H., Heland, J., Stohl, A., Forster,

C., Elbern, H. Jakobs, H., and Dickerson, R. R.: Global chemical weather forecasts for field campaign planning: predictions and observations of large-scale features during MINOS, CONTRACE, and INDOEX, Atmos. Chem. Phys., 3, 267–289, 2003, http://www.atmos-chem-phys.net/3/267/2003/.

Lelieveld, J., Butler, T. M., Crowley, J. N., Dillon, T. J., Fischer, H., Ganzeveld, L., Harder, H., Lawrence, M. G., Martinez, M., Taraborrelli, D., and Williams, J.: Atmospheric oxidation capacity sustained by a tropical forest, Nature, 452, 737–740, 2008.

Levy II, H.: Normal atmosphere: Large radical and formaldehyde concentrations predicted, Science, 173, 141–143, 1971.

Madronich, S. and Flocke, S.: The role of solar radiation in atmospheric chemistry, in Handbook of Environmental Chemistry, edited by: Boule, P., Springer, New York, 1–26, 1998.

Paulson, S. E. and Orlando, J.: The reactions of ozone with alkenes: An important source of HO_x in the boundary layer, Geophys. Res. Lett., 23, 3727–3730, 1996.

Paulson, S. E., Chung, M. Y., and Hasson, A. S.: OH radical formation from the gas-phase reaction of ozone with terminal alkenes and the relationship between structure and mechanism, J. Phys. Chem. A, 103(41), 8125–8138, 1999.

Poisson, N., Kanakidou, M., Crutzen, P. J.: Impact of non-methane hydrocarbons on tropospheric chemistry and the oxidizing power of the global troposphere: 3-dimensional modelling results, J. Atmos. Chem., 36, 157–230, 2000.

Preston, K. F. and Cvetanovic, R. J.: Collisional deactivation of excited oxygen atoms in the photolysis of NO_2 at 2288 Å, J. Chem. Phys., 45, 2888–2893, 1966.

Ren, X., Harder, H., Martinez, M., Faloona, I., Tan, D., Lesher, R. L., DiCarlo, P., Simpas, J. B., and Brune, W. H.: Interference testing for atmospheric HO_x measurements by laser-induced fluorescence, J. Atmos. Chem., 47, 169–190, 2004.

Ren, X., Olson, J. R., Crawford, J. H., Brune, W. H., Mao, J., Long, R. B., Chen, Z., Chen, G., Avery, M. A., Sachse, G. W., Barrick, J. D., Diskin, G. S., Huey, L. G., Fried, A., Cohen, R. C., Heikes, B., Wennberg, P. O., Singh, H. B., Blake, D. R., and Shetter, R. E.: HO_x chemistry during INTEX-A 2004: Observation, model calculation, and comparison with previous studies, J. Geophys. Res., 113, D05310, doi:10.1029/2007JD009166, 2008.

Sander, S. P., Friedl, R. R., Golden, D. M. Kurylo, M. J., Moortgat, G. K., Wine, P. H., Ravishankara, A. R., Kolb, C. E., Molina, M. J., Finlayson-Pitts, B. J., Huie, R. E., and Orkin, V. L.: Chemical kinetics and photochemical data for use in atmospheric studies, Evaluation Number 15, JPL Publication 06–2, NASA/Jet Propulsion Laboratory, Pasadena, California,

USA, 2006.
Sinha, V., Williams, J., Crowley, J. N., and Lelieveld, J.: The comparative reactivity method – a new tool to measure total OH reactivity in ambient air, Atmos. Chem. Phys., 8, 2213–2227, 2008, http://www.atmos-chem-phys.net/8/2213/2008/.
Stickler, A., Fischer, H., Bozem, H., Gurk, C., Schiller, C., Martinez-Harder, M., Kubistin, D., Harder, H., Williams, J., Eerdekens, G., Yassaa, N., Ganzeveld, L., Sander, R., and Lelieveld, J.: Chemistry, transport and dry deposition of trace gases in the boundary layer over the tropical Atlantic Ocean and the Guyanas during the GABRIEL field campaign, Atmos. Chem. Phys, 7, 3933–3956, 2007.
Thornton, J. A., Woolridge, P. J., Cohen, R. C., Martinez, M., Harder, H., Brune, W. H., Williams, E. J., Roberts, J. M., Fehsenfeld, F. C., Hall, S. R., Shetter, R. E., Wert, B. P., and Fried, A.: Ozone production rates as a function of NO_X abundances and HO_x production rates in the Nashville urban plume, J. Geophys. Res., 107, 4146 pp., doi:10.1029/2001JD000932, 2002.
von Kuhlmann, R., Lawrence, M. G., Pöschl, U., and Crutzen, P. J.: Sensitivities in global scale modelling of isoprene, Atmos. Chem. Phys., 4, 1–17, 2004, http://www.atmos-chem-phys.net/4/1/2004/.
Vranckx, S., Peeters, J., and Carl, S. A.: Absolute rate constant and $O(^3P)$ yield for the $O(^1D)+N_2O$ reaction in the temperature range 227 K to 719 K, Atmos. Chem. Phys. Discuss., 8, 8881–8912, 2008, http://www.atmos-chem-phys-discuss.net/8/8881/2008/.
Williams, J., Yassaa, N., Bartenbach, S., and Lelieveld, J.: Mirror image hydrocarbons from Tropical and Boreal forests, Atmos. Chem. Phys., 7, 973–980, 2007, http://www.atmos-chem-phys.net/7/973/2007/.

Table 1. Systematic errors for lamp flux calibration.

	1σ error
NO monitor (TECO)	6%
NO standard (NIST)	1%
Mass Flow Controllers (MKS)	2%
N_2O cross section σ_{N2O}	2%
$O(^1D)$ yield	1%
Kinetic rates	12%
Photolysis chamber dimensions	10%
Pressure sensor (MKS)	2%

ACPD
8, 15491–15536, 2008

Table 2. Precision and accuracy (1σ) of the HO_x measurements during GABRIEL.

1σ	OH	HO_2
Precision	7%	1%
Accuracy		
all data except flights #2 and #7	20%	30%
flights #2 and #7	30%	30%
Possible maximum under-estimation in the BL (or over-estimation in the FT)	50%	50%

ACPD
8, 15491–15536, 2008

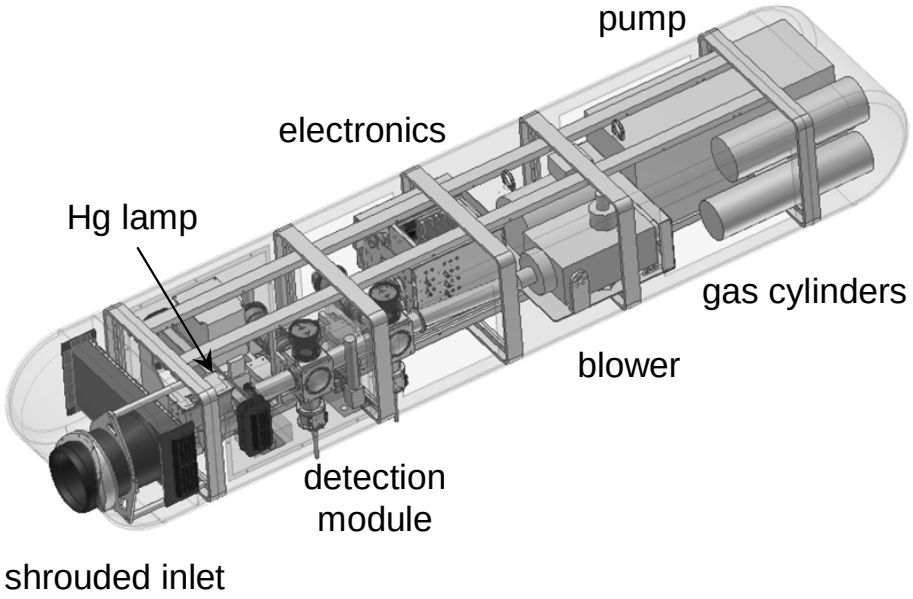

Fig. 1. Instrument setup in the wingpod.

ACPD
8, 15491–15536, 2008

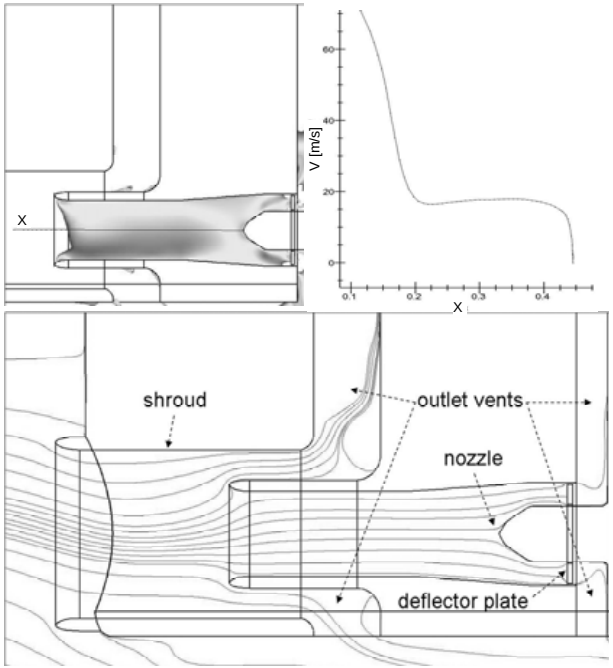

Fig. 2. Computational Fluid Dynamics calculations performed by H. Bijl and colleagues (Delft University). The velocity in the shrouded inlet is shown in the upper right panel, along the line indicated in the upper left panel. Streamlines in the shrouded inlet at an angle of attack of 15° are shown in the lower panel.

ACPD
8, 15491–15536, 2008

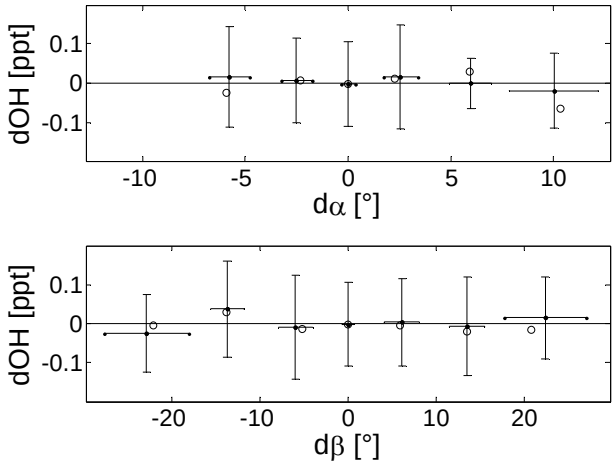

Fig. 3. Change in OH mixing ratio measured within the 10 s resolution of the instrument as a function of change in pitch (a) and roll (b), means (1σ error bars) and medians (open circles) of 3° bins for pitch and 7° bins for roll angle change. We only included data collected when the Learjet was initially flying at average angles ((5±3)° pitch and (0±7)° roll).

ACPD
8, 15491–15536, 2008

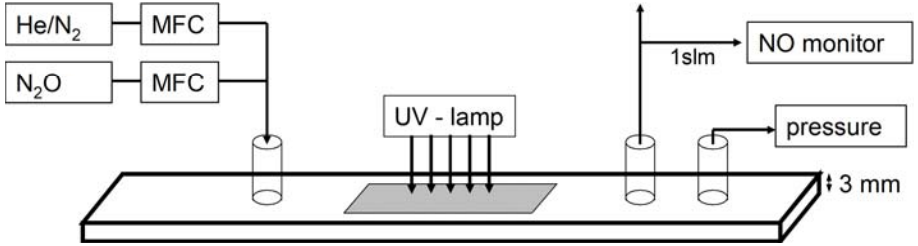

Fig. 4. Schematic representation of the photolysis chamber used for lamp flux calibration.

ACPD
8, 15491–15536, 2008

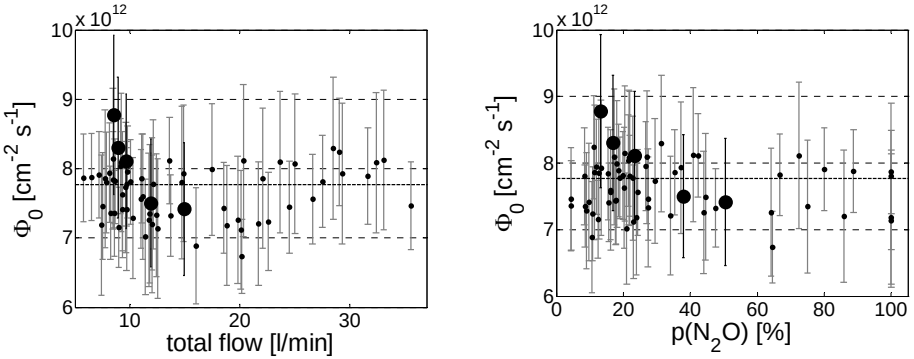

Fig. 5. Photon fluxes derived from NO yields from irradiation of N_2O at different flow rates (left panel) and with different mixing ratios of N_2O (right panel) in helium (small symbols) and nitrogen (large symbols).

ACPD
8, 15491–15536, 2008

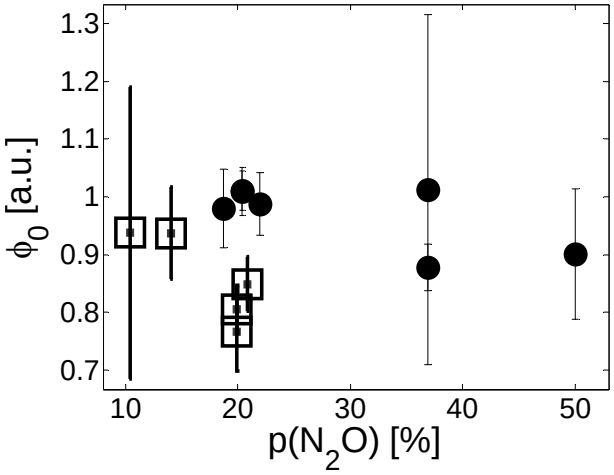

Fig. 6. Lamp flux measured with 3 mm photolysis chamber (solid circles) and with the calibration tube with a 50 slm flow (open squares).

ACPD
8, 15491–15536, 2008

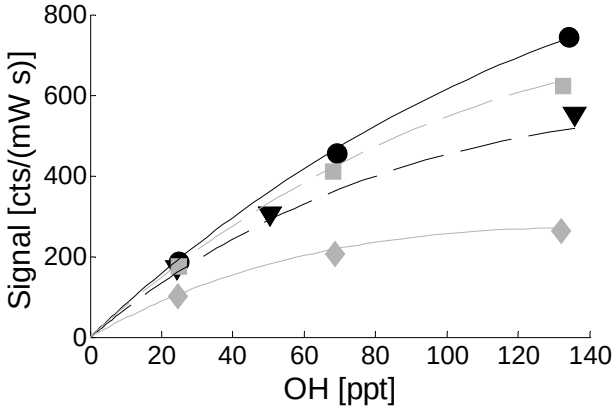

Fig. 7. Ground calibration performed during the campaign. Different OH concentrations were produced by irradiation of air with varying humidity, and the signal recorded at various internal pressures (black circles at 2 hPa, grey squares at 3.1 hPa, black triangles at 4.6 hPa, diamonds at 8.3 hPa).

ACPD
8, 15491–15536, 2008

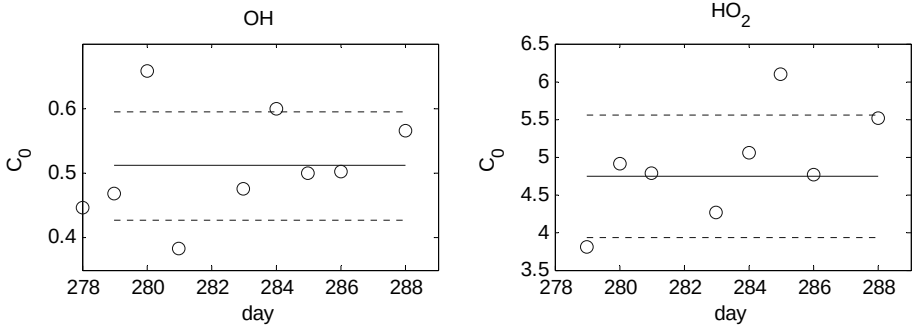

Fig. 8. Parameters C_0 derived from ground calibrations during the campaign. The time is indicated as Julian day, the solid line shows the mean value and the dashed lines the 1σ standard deviation.

ACPD
8, 15491–15536, 2008

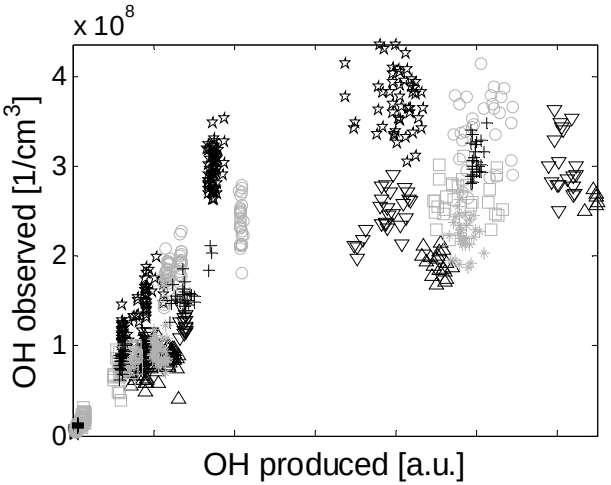

Fig. 9. In-flight calibrations (different symbols for each flight) evaluated according to the sensitivities derived from ground calibrations.

ACPD
8, 15491–15536, 2008

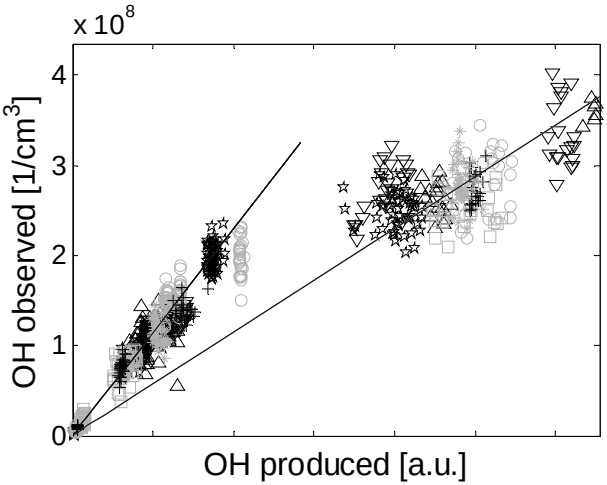

Fig. 10. In-flight calibrations (different symbols for each flight). Each flight was evaluated using the sensitivities derived from ground calibrations corrected by a constant factor for each flight in order to achieve best agreement of all flights. Seemingly two different sensitivity regimes exist, with higher sensitivity in conditions where less OH is produced by the in-flight calibrator.

ACPD
8, 15491–15536, 2008

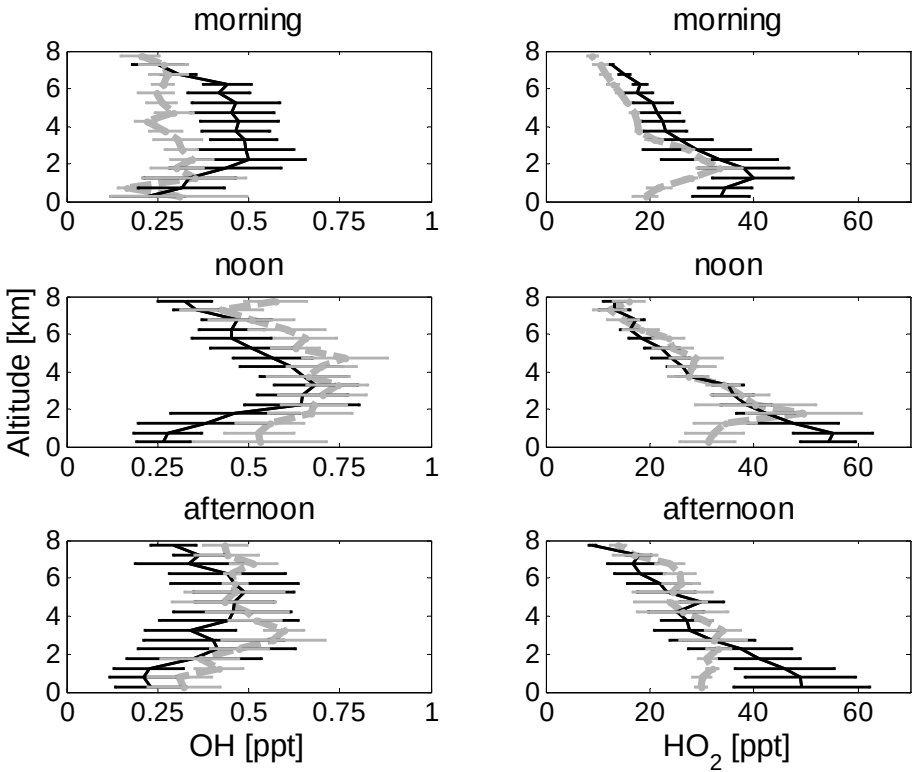

Fig. 11. Average profiles of OH and HO_2 mixing ratios over the ocean (grey dashed lines) and over the forest (black solid lines) measured in the morning (08:00–11:00 LT), around noon (11:00–14:00 LT) and in the afternoon (14:00–17:00 LT).

ACPD
8, 15491–15536, 2008

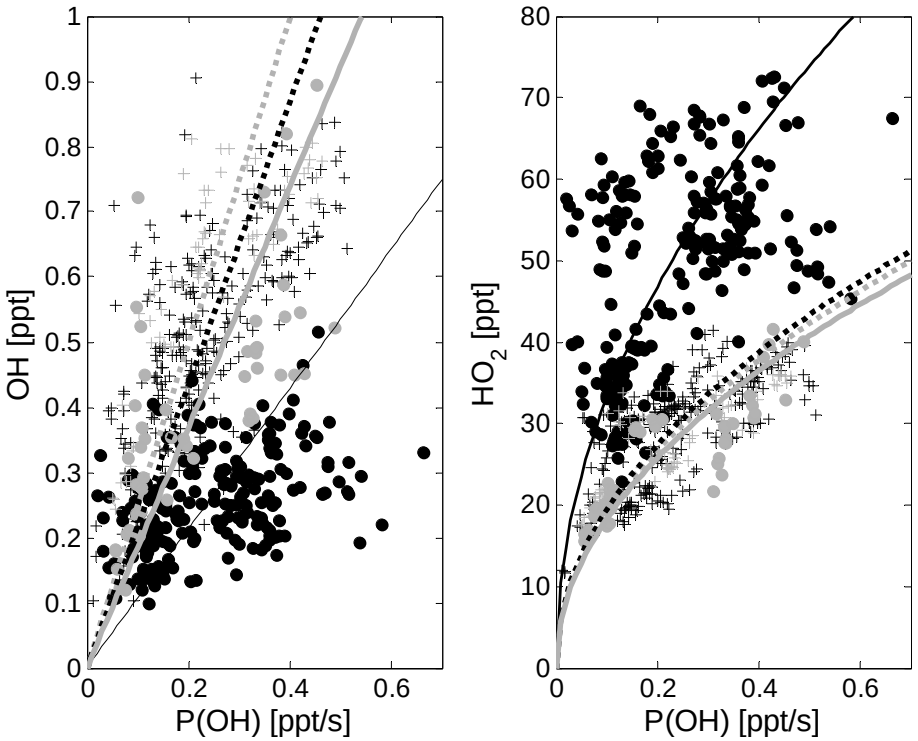

Fig. 12. Mixing ratios of OH and HO_2 as a function of OH production from photolysis of O_3 in the free troposphere between 3000 and 5000 m a.s.l. (crosses, dotted lines) and below 1000 m a.s.l. (solid circles, solid lines) over the forest (black) and over the ocean (grey).

ACPD
8, 15491–15536, 2008

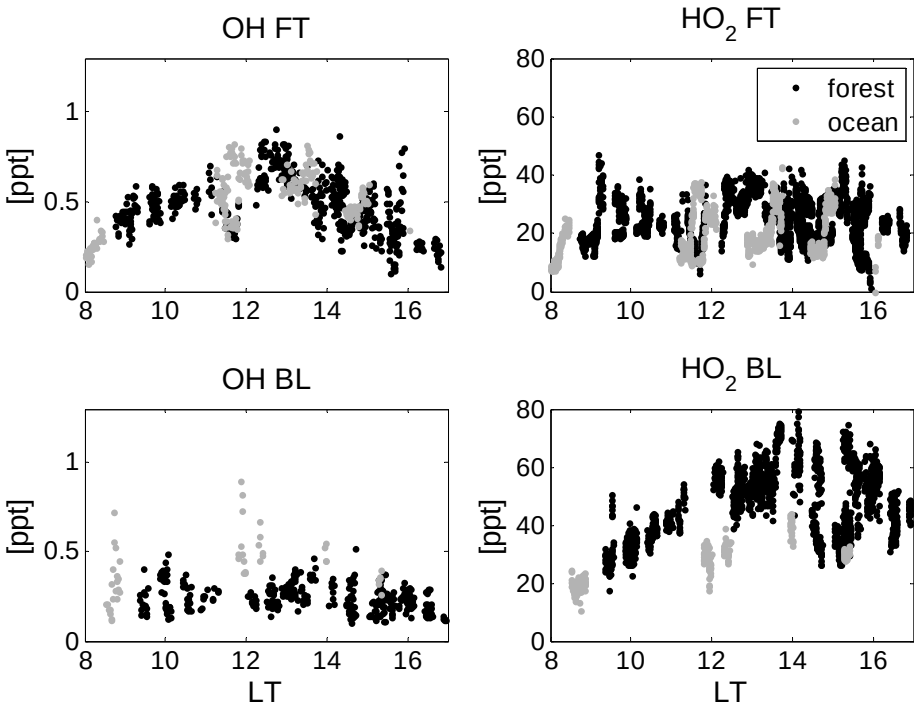

Fig. 13. Diurnal variation of OH (1 min data) and HO_2 (10 s data) above 3000 m a.s.l. (free troposphere, FT) and below 1000 m a.s.l. (boundary layer, BL) over the forest (black) and over the ocean (grey).

ACPD
8, 15491–15536, 2008

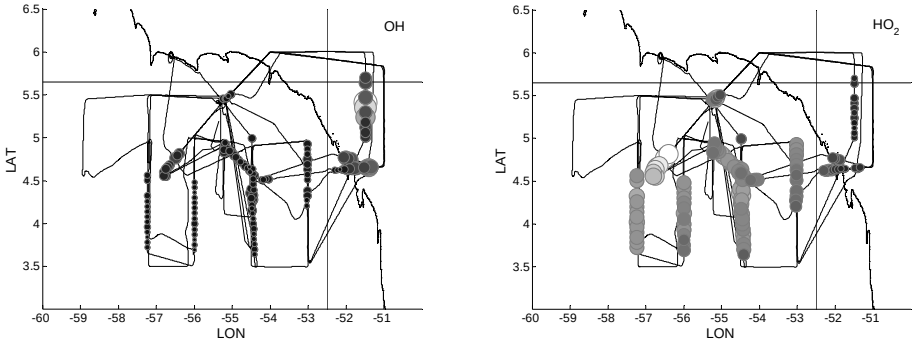

Fig. 14. Geographical distribution of OH (left panel) and HO_2 (right panel) in the lowest 1000 m a.s.l. measured around noon (11:00–14:00 LT). Mixing ratios are represented by circle diameters as well as color (lighter for higher mixing ratios). The location of the coastline and the flight tracks are also shown (black lines).

ACPD
8, 15491–15536, 2008

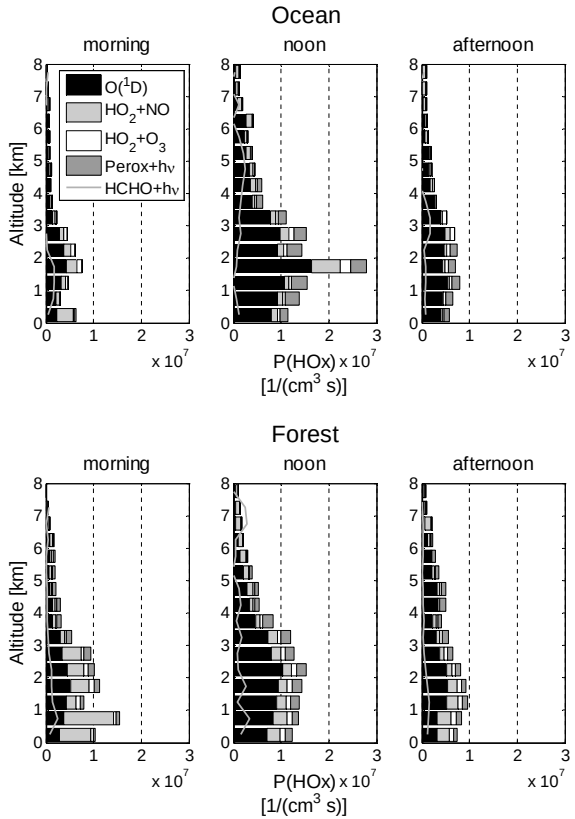

Fig. 15. Median profiles of the main OH production rates calculated from measured trace gas concentrations over the ocean (upper row) and over the forest (lower row) measured in the morning (07:00–11:00 LT), around noon (11:00–14:00 LT) and in the afternoon (14:00–17:00 LT). In addition, the production of HO_2 via photolysis of formaldehyde is shown by the grey line.

ACPD
8, 15491–15536, 2008

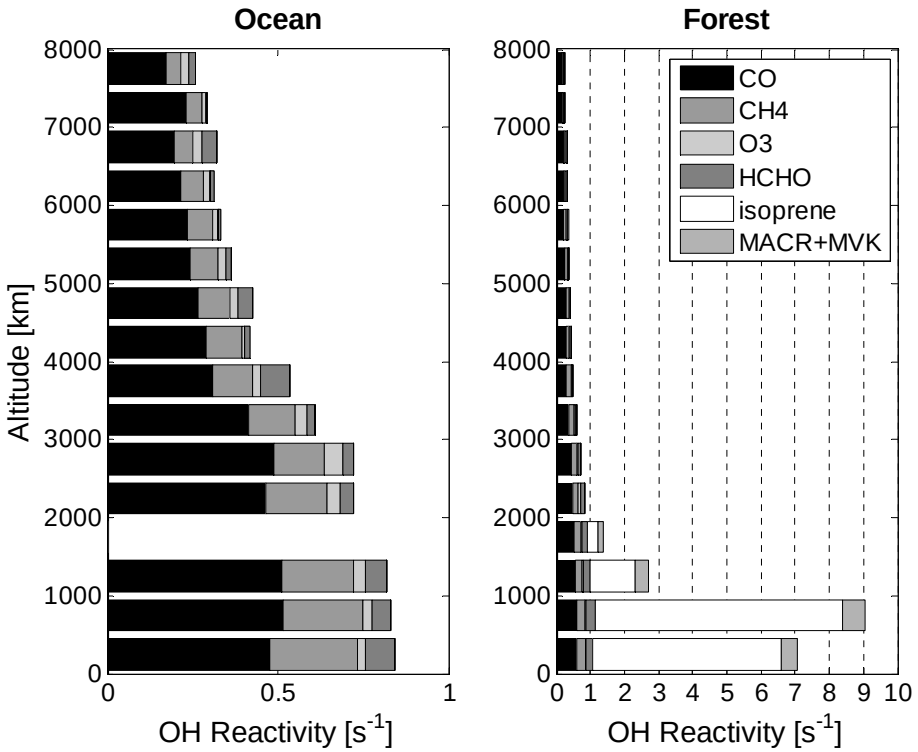

Fig. 16. Median profiles of the dominant reactions contributing to total OH loss, calculated from measured trace gas concentrations over the ocean (left panel) and over the forest (right panel), columns stacked in the order given in the legend.

ACPD
8, 15491–15536, 2008

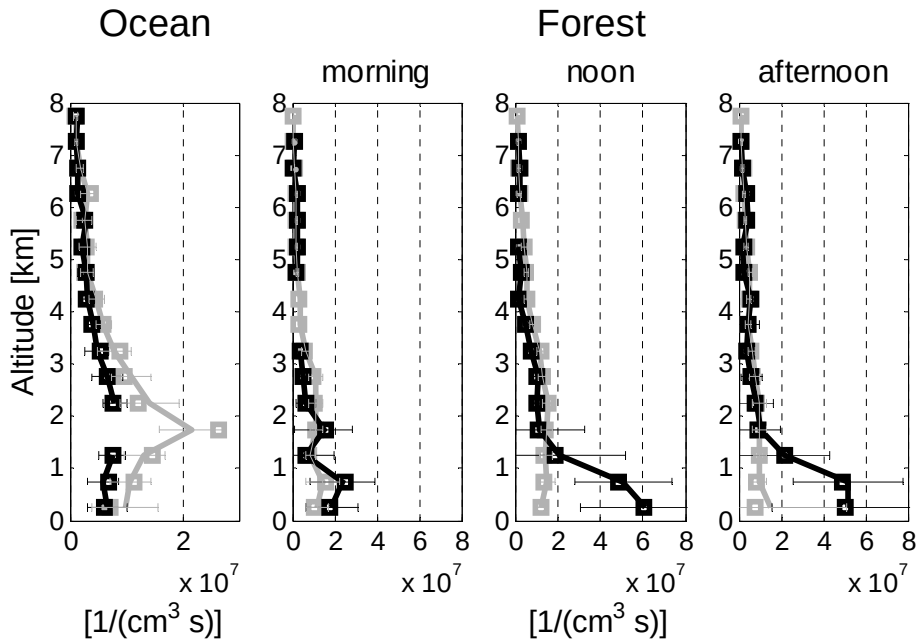

Fig. 17. Mean profiles of OH production (grey) and destruction (black), over the ocean (all data) and over the forest at different times of day. The squares indicate the median values, the error bars the variability (standard deviation).

ACPD
8, 15491–15536, 2008

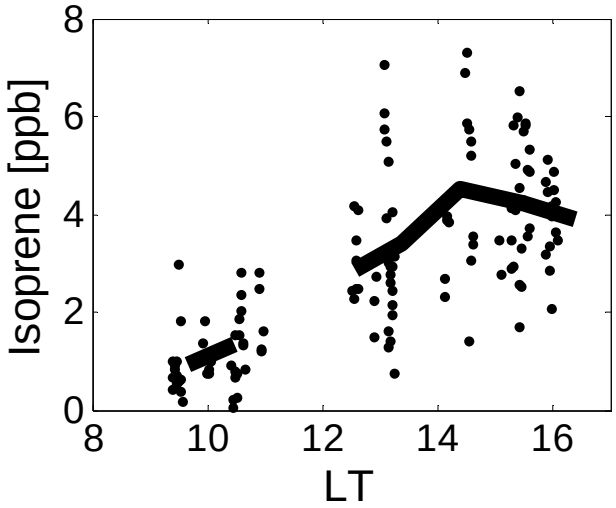

Fig. 18. Diurnal variation of isoprene in the forest boundary layer (below 1000 m a.s.l.).

ACPD
8, 15491–15536, 2008